CEAS Aeronautical Journal
https://doi.org/10.1007/s13272-025-00888-1

ORIGINAL PAPER

Parametric approach to primary structure modeling of aircraft for cabin noise analysis in FEM

R. D. Dewald[1] · T. Klimmek[1] · C. Hesse[2] · R. Winter

Received: 16 March 2025 / Revised: 21 July 2025 / Accepted: 7 August 2025

Abstract
The goals of the European Green Deal require the development of low-emission aircraft propulsion systems that consider sustainable fuels. However, there is a conflict of objectives between effective fuel reduction and noise development of the propulsion system, as particularly efficient propulsion concepts are often based on open rotors, which usually cause increased exterior and interior noise. As a result, precise vibroacoustic models are essential in the early design phase to evaluate and mitigate cabin noise. However, many essential details required for accurate cabin noise prediction are not yet fully defined during preliminary aircraft design. Consequently, the simulation chain consisting of the excitation, primary structure, secondary structure and cavity contains numerous assumptions. To address this challenge, this publication focuses on the parametric creation of full primary structure models based on preliminary design data, with a level of detail relevant for the vibroacoustic frequency range. A central contribution of this work is the derivation of generic modeling guidelines, such as wave-resolving element discretization in the circumferential direction and longitudinal direction of the fuselage structure as well as parameterization of rivet stiffness, from high-resolution experimental vibration data from the research platform Acoustic Flight-Lab. These guidelines are applicable to other fuselage configurations and aim to improve the accuracy of automated FE models. In addition to model creation, this publication proposes an approach for early vibroacoustic assessment at the primary structure level, utilizing spatially and spectrally integrated energy distributions. The applicability of this approach is demonstrated on two different aircraft configurations using realistic operating excitations of V2500 engines in cruise flight.

Keywords Aircraft interior noise · Sound transmission · Automated modeling · FEM

1 Introduction

The noise in the aircraft cabin is caused by various acoustic and vibrational sources, which are generated by aerodynamic effects, engine noise, engine vibrations and vibrations and noise from various systems within the aircraft. A dominant noise source is the turbulent boundary layer (TBL) on the fuselage surface, which is created by the air flow along the aircraft fuselage. This interaction leads to wall vibrations, which ultimately radiate into the cabin as noise. Another significant factor is the engine, which contributes both directly and indirectly to noise generation in the cabin. Acoustically, two types of engine noise are particularly relevant. The first is tonal fan noise, and the second is broadband jet engine noise. Despite technological advances in engine development, these noise sources remain a significant factor influencing cabin comfort. In addition to the acoustic noise sources, there are also vibrational sources in the engine that significantly contribute to cabin noise. Imbalances in the engine lead to vibrations that propagate to the fuselage as structure-borne noise and result in sound radiation within the cabin. Modern propulsion concepts, particularly their higher sheath flow ratios, are characterized by larger rotating masses at lower engine speeds, which leads to an increase in engine-induced vibrations at lower frequencies, thus contributing to better propagation.

To enable sufficiently accurate cabin noise prediction of new aircraft configurations already in the aircraft design phase, it is necessary to quantify the individual noise and vibration sources as well as to accurately model the entire transfer path between the excitation and resulting sound

✉ R. D. Dewald
ray.dewald@dlr.de

[1] German Aerospace Center (DLR), Institute of Aeroelasticity, Göttingen, Germany

[2] German Aerospace Center (DLR), Institute of System Architectures in Aeronautics, Hamburg, Germany

Published online: 22 August 2025

pressures in the cabin. This requires an overall aircraft model in which the primary structure is interconnected with the secondary structure and the cavity, on the basis of which the calculation of the aircraft interior noise is carried out [1]. In this context, an automated model setup of the entire aircraft supports the rapid integration of modifications for a comparative noise assessment. The simulation chain described here for calculating the cabin noise is shown as an example for a surface pressure excitation in Fig. 1.

In the overall modeling of the aircraft, the primary structure is the central node in the transmission path of airborne and structure-borne noise into the aircraft cabin. The pressure fluctuations of all external noise sources are projected onto the fuselage surface as imprinted forces in the form of distributed loads and cause it to vibrate. The airborne noise from the engine first passes through the turbulent boundary layer before it affects the fuselage skin. The vibrations of the fuselage structure are then transmitted to the elements of the cabin interior, whereas engine vibrations are transmitted via the primary structure as structure-borne sounds and thus also reach the cabin area.

The primary objective of the present work is to establish generic modeling guidelines for the parametric creation of complete primary structure models in the mid-frequency range, with the aim of improving the prediction accuracy of automatically generated finite element (FE) models. For this purpose, these guidelines are derived from high-resolution measured data (12,000 positions) from the research platform Acoustic Flight-Lab (AFL), which represents a simplified A320 fuselage structure [2] and serves as a reference for other modeling guidelines developed in previous studies [3]. To date, the wave-resolving discretization of primary fuselage structure models has been based on the minimum bending wavelength derived from the assumption of an infinite plate [4] [5]. Accordingly, Sect. 2 proposes a functional expression for the minimum bending wavelength up to 500 Hz, derived from a wavenumber analysis. In addition, updated stiffness parameters for rivet modeling in fuselage structures are presented as an additional modeling guideline.

Section 3 extends the primary structure modeling using the example of an overall aircraft configuration. Additionally, the characterization of the operating loads of a V2500 engine during cruise flight is addressed.

In Sect. 4, an energy-based approach at the primary structure level is proposed, allowing early assessment of the structural characteristics of the aircraft in an effective and condensed way. Structural modifications in the early phases of the design process of aircraft, such as the optimization of stringer and frame layouts [6], can be examined on a fuselage level along with static structural sizing [7]. Options that exhibit significant structural weaknesses at the primary structure level that were not present in the original configuration can be down-selected and excluded

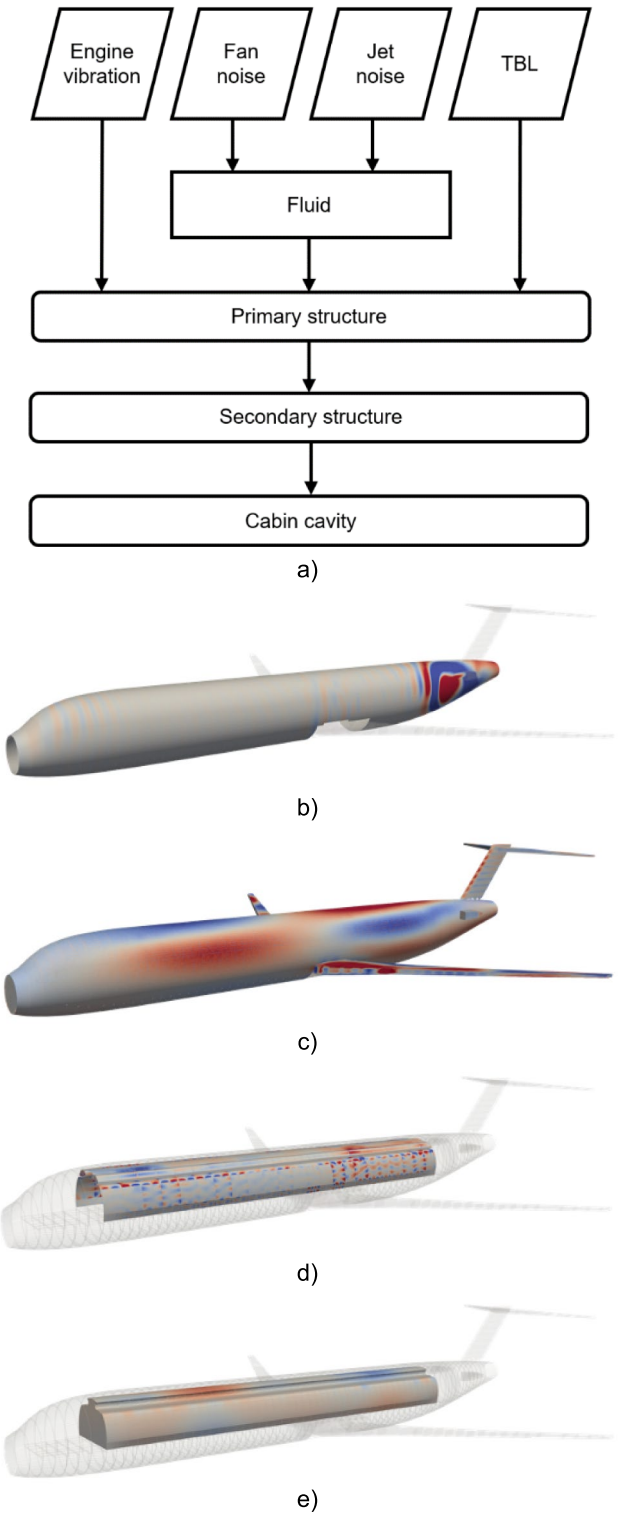

Fig. 1 Simulation chain for calculating cabin noise (excitation of fan noise at 86 Hz): **a** flow chart of the simulation chain including the most relevant acoustic and vibrational sources, **b** complex surface pressure excitation, **c** vibration of the primary structure, **d** vibration of the cabin cladding (secondary structure), **e** sound pressure in the cabin

from further analysis through the full FEM simulation chain, which requires an adaptation of the secondary structure to the altered primary structure, thus leading to a more time-efficient design process. Section 5 concludes the paper with a final discussion.

2 Modeling guidelines

This chapter addresses the parametric modeling of primary fuselage structures in detail, including validated modeling guidelines for the construction of primary structure models, which can be used, particularly for model generators, to generate overall aircraft models for vibroacoustic analyses.

2.1 Parametric modeling concept

The model generator ModGen [8] developed at the DLR Institute of Aeroelasticity has been extended in recent years and is now able to automatically generate complete FE structural models for vibroacoustic analyses from parametric design data stored in the CPACS format [9] (Common Parametric Aircraft Configuration Schema). Its standard output is datasets for the FE solver NASTRAN. The design data contain the necessary information on the material and geometric properties of the aircraft, such as the exact position of the stiffening fuselage elements (stringers, frames) and their corresponding profile cross-sections. Unlike models for load analysis, models for vibroacoustic analyses must be modeled with a comparatively high level of detail. For example, the stiffeners in the fuselage and floor structure are not modeled with simple beams and rods but with linear shell elements corresponding to the profile cross section (see Fig. 2).

To ensure that the vibroacoustic properties of the primary structure model are closer to reality, even the smallest details, such as the rivets, are modeled. One approach to modeling rivets involves CFAST elements. The use of CFAST elements not only allows relevant local stiffness, damping and mass effects to be taken into account but also eliminates modeling restrictions such as the connection of adjacent components (e.g., cross beams to frames) via coincident nodes. This allows flexible modeling, while the positions of all the components stored in the CPACS file are maintained. In the case of a connection via coincident nodes, for example, the position of these components would inevitably shift depending on the mesh resolution. Overall, this modeling concept allows the automated construction of an FE model at the component level and offers the possibility of setting mesh refinement parameters.

The stiffness parameters of the CFAST elements were optimized as part of model updating so that the difference between the experimentally and numerically identified natural frequencies is minimal. Matching mode pairs between the simulation and experiment were identified via the modal assurance criterion. Figure 3 shows an exemplary vibration mode of the AFL structure, which was used for updating. A total of 16 modes in a frequency range of up to 100 Hz were considered in the optimization process. Model updating was carried out in NASTRAN via Solution 200, which is a gradient-based optimization method. The optimized stiffness values can be found in Table. 1.

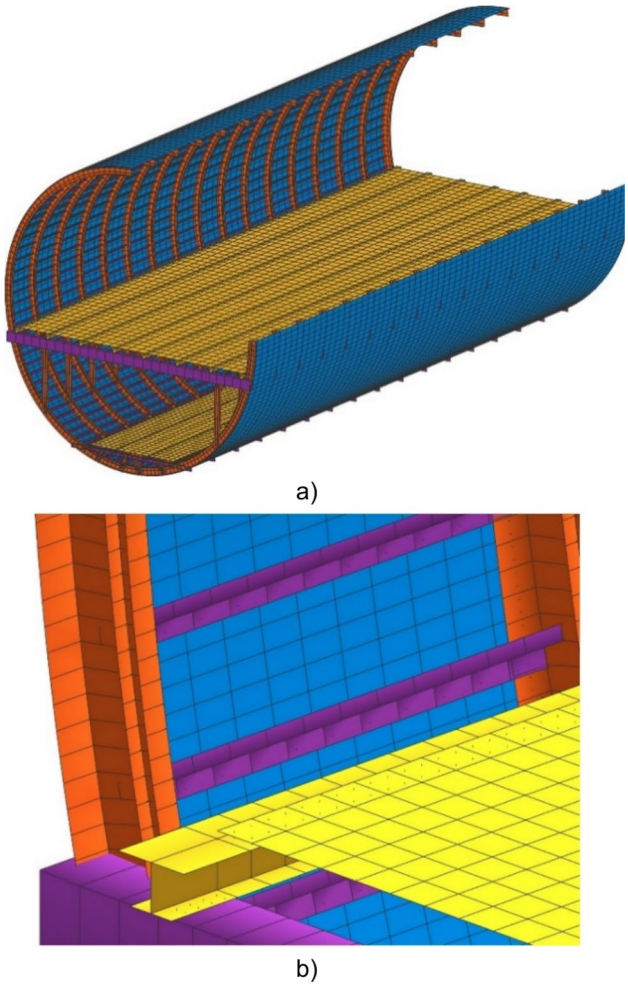

Fig. 2 Overview of the AFL FE model: **a** three-quarter section view, **b** close-up view (black dots in the model represent the CFAST elements)

The updated stiffness parameter values of the CFAST elements, obtained via model updating using high-resolution vibration measurements of the AFL structure, represent more realistic stiffening characteristics in fuselage structures and can be transferred to other configurations. In the updated fuselage model, CFAST elements are equally spaced along the component interfaces (see Table 2), locally introducing a defined amount of additional stiffness. Applying the same spacing in other fuselage structures allows for a comparable improvement in vibration behavior. This modeling guideline

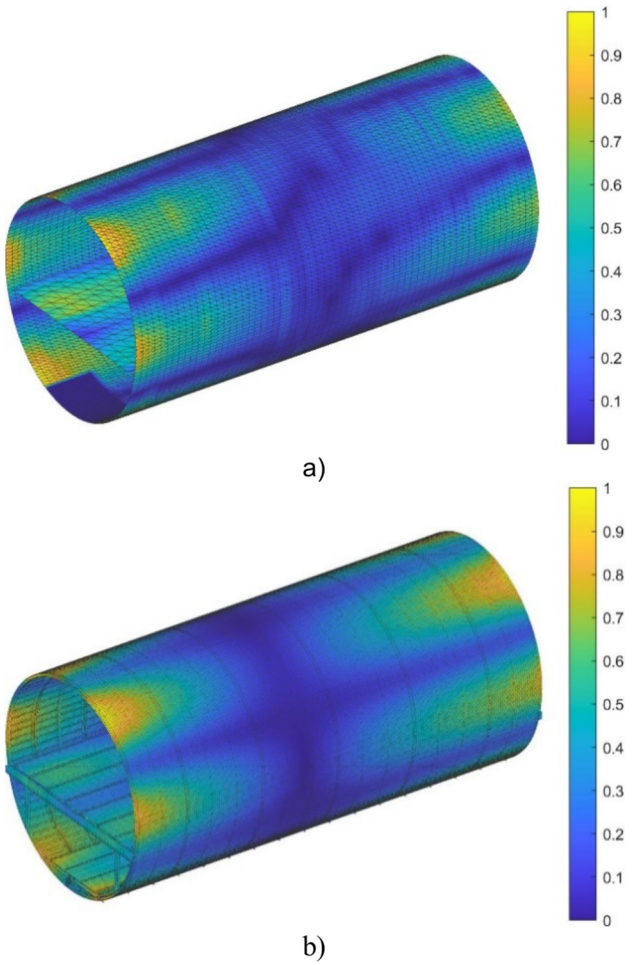

Fig. 3 Mode comparison (normalized displacement): **a** experiment @ 33.2 Hz, **b** FEM @ 33.4 Hz

Table 1 Optimized CFAST stiffnesses: KT denotes translational stiffness, and KR denotes rotational stiffness

Property	Value	Unit
KTX	$2.712 \cdot 10^6$	N/m
KTY	$4.598 \cdot 10^5$	N/m
KTZ	$1.288 \cdot 10^5$	N/m
KRX	6398.22	N/m
KRY	48.4389	N/m
KRZ	29.4158	N/m

Table 2 CFAST layout of the optimized AFL model

Interface	Lining	Spacing	Unit
Frame/skinfield	single	0.012	m
Stringer/skinfield	single	0.022	m
Beam/floor panel	double	0.041	m

is particularly suited for fuselage structures where no experimental data are available for model updating, such as configurations based on preliminary design data. The deterministic nature of this approach provides a robust foundation for predictive modeling.

Based on the discretization of the fuselage model, the spacing of the CFAST elements can be adjusted accordingly, as the stiffness values scale linearly while largely preserving their characteristic behavior. It is recommended to place at least one CFAST element per finite element patch.

2.2 Wavenumber-based mesh resolution

Wavenumber analysis is a method for investigating the spatial vibration distribution of a structure. It uses the 2D Fourier transformation to transfer operational deflection shapes $u(x, y)$ from the spatial space to the wavenumber space $\hat{u}(kx, ky)$.

$$\hat{u}\left(k_x, k_y\right) = \iint u(x, y) e^{-\mathrm{i}\left(k_x x + k_y y\right)} \, dx \, dy \tag{1}$$

Here, the wavenumbers kx, ky indicate the spatial frequency components of the oscillation. As experiments and the finite element method (FEM) provide discrete measuring points, discrete implementations of the Fourier transform are used in practical realization. In [10], it is shown that this method is particularly suitable for the investigation of structures with high modal density, as the analysis of wavenumbers enables a systematic separation of different vibration patterns. The presence of both low and high wavenumbers at a discrete frequency indicates that the structure exhibits global as well as local behavior.

The correct choice of mesh resolution is highly important for FE models used for vibroacoustic analyses. While according to the Nyquist-Shannon sampling theorem, only slightly more than two points per wavelength are necessary to identify the corresponding frequency, studies have shown that at least 6 to 10 linear elements per occurring wavelength are required in the FE model to adequately represent structure-borne sound propagation [11–13]. Particularly in large structures, such as aircraft, very high mesh resolutions lead to unnecessarily long computing times with very extreme resource consumption at the same time. To prevent excessively fine mesh resolutions from being used when creating primary structure models of aircraft, an extensive spatial wavenumber analysis was carried out using the experimentally measured vibration data from the AFL. These measurement data serve as a suitable basis for determining the frequency-dependent wavenumbers occurring on the aircraft fuselage, which can then be incorporated as reference values in the parametric model generator to automatically generate

suitable mesh refinement depending on the frequency range application.

The wavenumbers identified by the Fourier transform in both the circumferential and longitudinal directions of the fuselage are shown in Fig. 4. With the experimental measurement grid configuration used for the fuselage surface, the occurring wavenumbers could be identified up to 500 Hz in the longitudinal direction and up to 450 Hz in the circumferential direction. Beyond these frequency limits, it was no longer possible to spatially resolve higher wavenumbers. Compared with the longitudinal direction of the fuselage, significantly higher wavenumbers occur in the circumferential direction from approx. 155 Hz. The sudden occurrence of higher wavenumbers indicates local vibration phenomena, which result in particular from the fuselage stiffeners. Biedermann [10] classifies the mid-frequency range from this point onward, which is characterized by the superposition of local and global vibration modes.

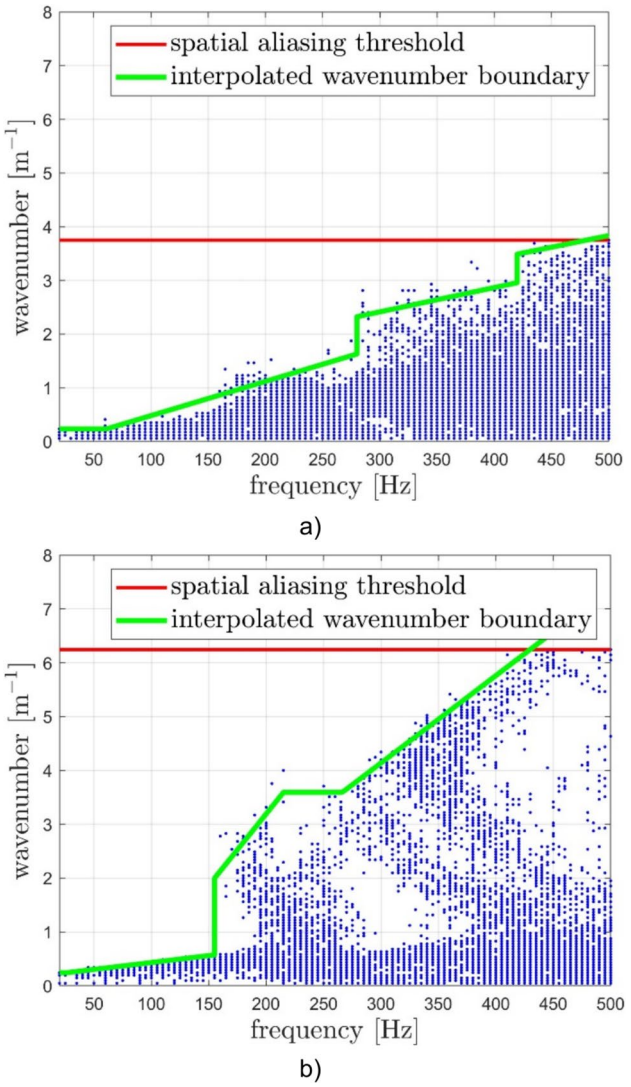

Fig. 4 Wavenumber analysis of the experimentally measured operational deflection shapes; identified wavenumbers are represented by the blue dots: **a** in the circumferential direction of the fuselage and **b** in the longitudinal direction of the fuselage

The maximum wavenumbers are decisive for the choice of mesh resolution. To describe this information with minimum complexity and thus make it more useful for model generators in particular, the maximum wavenumber k_{max} was approximated as a function of the frequency f via piecewise interpolation that preserves monotonicity (green line). The parameters were determined using the method of least squares. The functional relationship can be expressed in the longitudinal direction of the fuselage as

$$k_{max}(f) = \begin{cases} 0.2265 & ,f = [20, 60[\\ 0.0064 \bullet f - 0.1563 & ,f = [60, 280[\\ 0.0045 \bullet f + 1.0566 & ,f = [280, 420[\\ 0.0043 \bullet f + 1.6774 & ,f = [420,500] \end{cases} \tag{2}$$

and in the circumferential direction of the fuselage as

$$k_{max}(f) = \begin{cases} 0.0026 \bullet f + 0.1760 & ,f = [20, 155[\\ 0.0266 \bullet f - 2.1233 & ,f = [155, 215[\\ 3.6 & ,f = [215, 265[\\ 0.0162 \bullet f - 0.6930 & ,f = [265, 450] \end{cases}. \tag{3}$$

The limits of the interpolation ranges were defined at positions where the rate of change $\Delta k_{max}/\Delta f$ between successive measurement points exceeds a defined threshold TH

$$TH = \bar{s} + k \bullet \sigma_s \tag{4}$$

where $\bar{s}$ is the mean value of the rates of change, σ_s is the standard deviation of the rates of change, and k is an empirically selected scaling factor. Here, $k = 4$ was chosen to detect larger changes in the wavenumber curve.

A comparison with the results of the wavenumber analysis based on the simulated operating deflection shapes (see Fig. 5) reveals that the characteristic curves of the frequency-dependent wavenumbers are very similar. In particular, the maximum wavenumbers occurring between the experiment and simulation are almost of the same order of magnitude; only slightly higher wavenumbers occur in the FE model at higher frequencies. Minor deviations in the wavenumber analysis can be explained by possible leakage effects during the transformation, as well as by the fact that the real AFL structure, in contrast to the FE model, does not have perfect symmetry, which can result in further local vibration phenomena that are not covered by the model. Overall, the comparison shows good agreement between experiment and simulation, which indicates that the applied modeling guidelines for creating the fuselage primary structure are suitable for performing vibroacoustic analyses.

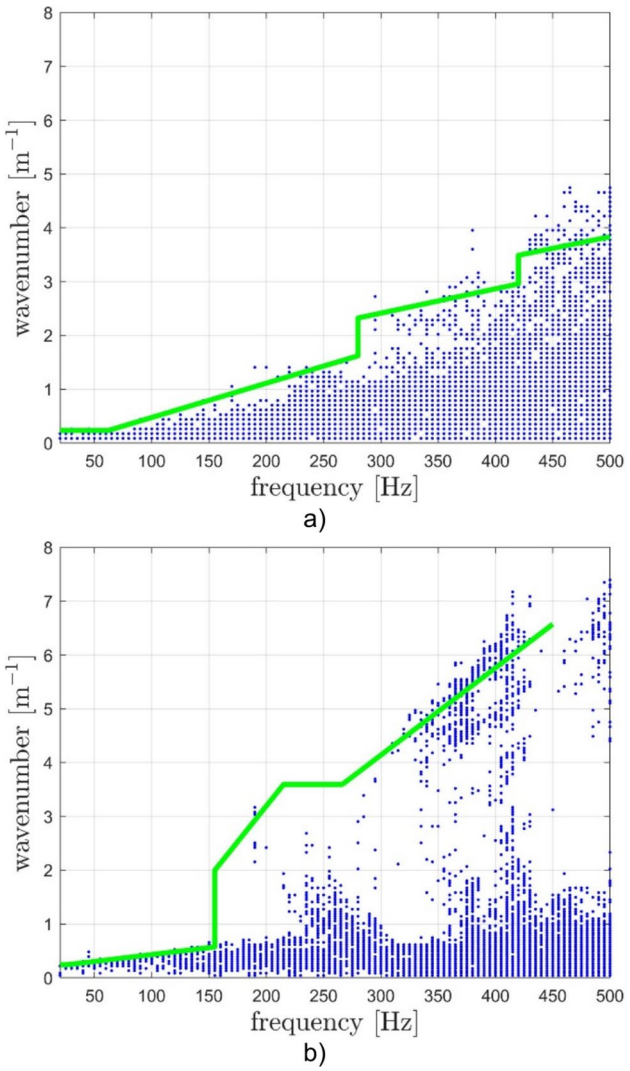

Fig. 5 Wavenumber analysis of the simulated operational deflection shapes; interpolated wavenumber boundary from Fig. 4 as a reference: **a** in the circumferential direction of the fuselage, **b** in the longitudinal direction of the fuselage

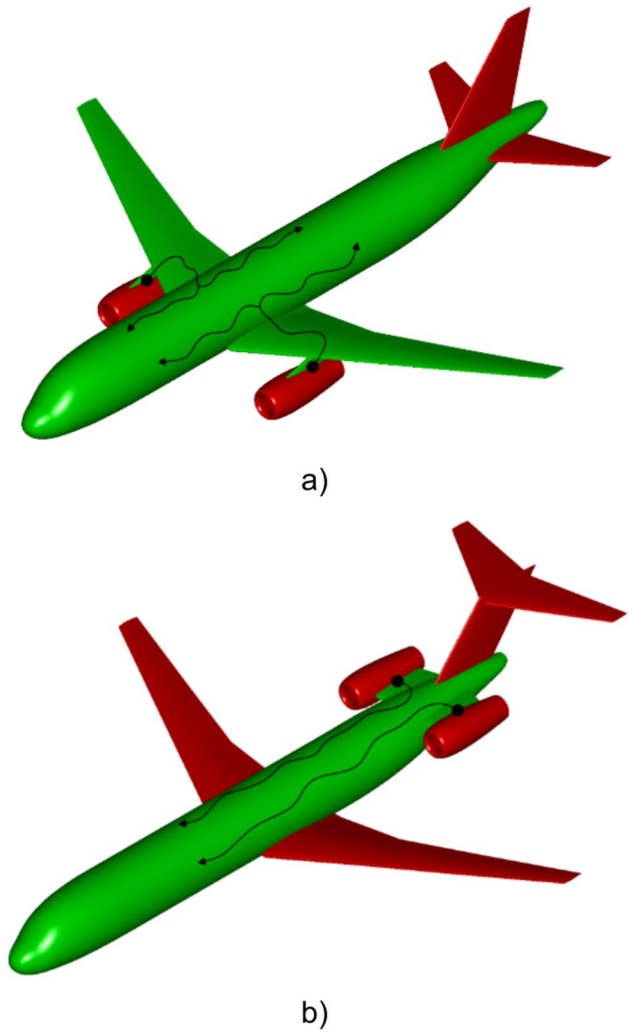

Fig. 6 Visualization of the aircraft configurations in the TiGL Viewer **a** D180 airplane configuration, **b** D180T aircraft configuration; the focus of the modeling depends on the structure-borne noise path of the engine vibrations (black line) relevant for cabin noise (green area = important, red area = of secondary importance)

3 Overall aircraft configuration

This section provides a summary overview of the two overall aircraft configurations, whose qualitative vibroacoustic properties are analyzed comparatively in the following chapter via a statistical energy distribution. The overall aircraft configurations are D180 and D180T, which are used in the DLR project INTONATE [14]. A schematic visualization of the basic structure and proportions of these configurations is shown in Fig. 6.

The two configurations differ fundamentally in the engine arrangement and the design of the tail assembly. In the D180 configuration, the engine is located underneath the wing, whereas in the D180T configuration, the engine is installed at the rear. In accordance with the cause-effect relationship, a specific excitation was simulated for both configurations. The excitation is composed of acoustic, fluid mechanical and vibratory sources, which are applied to the structural model as surface loads on the fuselage and as local forces on the engine−pylon interface, respectively.

3.1 Primary structure

The primary structure design of the two aircraft configurations was created on the basis of the associated CPACS datasets. The modeling guidelines from chapter 2 were used for the fuselage structure. In contrast to the AFL, other structural components relevant for vibroacoustic analysis must be modeled in addition to the main stiffening elements of the

fuselage skin and the inner beam structure for the passenger and cargo decks.

This includes the complex center fuselage area, which is responsible for holding the right and left wings (see Fig. 7b). For this purpose, a series of assemblies are defined in the CPACS dataset, which are used to attach the central wing box. The structural connection between these components is achieved not only via the same meshing rules but also via stiff connecting elements (RBE2), e.g., at the interface between the wing box and the vertical strut of the passenger deck. This ensures that all physically relevant transfer paths between the wing and fuselage are covered. This is necessary to analyze the influence of engine vibrations in an underwing configuration on the resulting cabin noise with sufficient accuracy. Furthermore, this meshing strategy favors the automated integration of the wing into the fuselage structure.

Equally important for vibroacoustic analyses, especially for rear engine mounting, is the integration of the pressure bulkheads (see Fig. 7c) because they reduce the transmission of aerodynamic and engine-induced noise into the cabin. The rear pressure bulkhead is connected to the fuselage skin via coincident nodes at the edges of the component. In this case, a refinement strategy avoids unnecessarily fine FE modeling and ensures good element quality without violating the continuity requirement of the displacement state.

3.2 Engine excitation

A wide variety of sources contribute to cabin noise, which can differ depending on the propulsion system and engine integration. The quantification of the source strengths and thus the significance of these contributions to the resulting cabin noise is crucial here.

The overall aircraft configurations presented are equipped with V2500 jet engines. The associated specific excitation sources are tonal fan noise, broadband jet noise and tonal engine-induced vibrations resulting from imbalances in low- and high-pressure shafts. In this publication, the acoustic noise sources, i.e., fan noise and jet noise, are used for the comparative analysis of the aircraft configurations. For this purpose, the DLR Institute of Aerodynamics and Flow Technology has provided surface pressure data with high temporal and spatial resolutions for the D180 and D180T configurations. The pressure fluctuations on the fuselage caused by the engine-generated fan noise are computed with the acoustic propagation solver DISCO++ [15]. The pressure fluctuations on the fuselage resulting from the broadband jet engine noise are simulated with the solver PIANO in combination with the stochastic source module FRPM using Tam & Auriault's jet noise model [16, 17]. The numerical calculations were carried out for a cruising speed of Ma=0.78, taking into account the turbulent boundary layer.

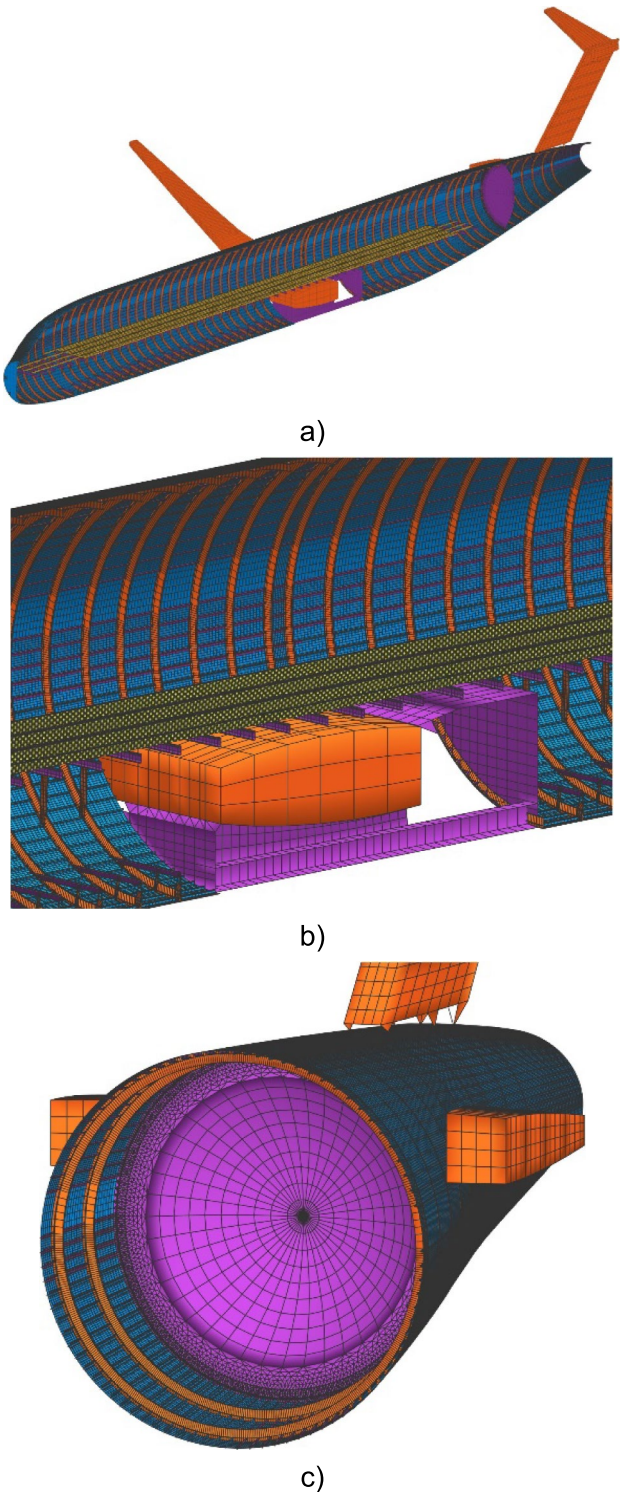

Fig. 7 D180T FE model overview: **a** half-view, **b** detailed view of the fuselage center section, **c** detailed view of the rear pressure bulkhead

The estimation of engine vibrations for the D180 configuration is covered in detail in [18]. Therefore, this section covers the fan noise and the jet noise in more detail in the

following, as there is no publication on these excitations for the aircraft configurations discussed here.

To make the surface pressure data of the respective excitation sources usable for the FE models of the D180 and D180T configurations, a linear interpolation was first carried out on the FE mesh to obtain a consistent pressure signature and thus avoid potential numerical artifacts in the FE calculations. The time data were then transformed to the frequency domain via Fourier transformation. Fig. 8 shows the corresponding result of the spectral analysis of the configuration-specific surface pressure data in the frequency range up to 500 Hz.

The fan noise up to 500 Hz contains the low-frequency tonal components of the Buzz Saw Noise, whose pressure signature is characterized by sharp wave fronts (see Fig. 1b). The fundamental harmonic of this noise depends on the fan's rotational frequency, which is approximately 86 Hz. In addition to the fundamental harmonic, the higher harmonics are also included in the surface pressure excitation, which decreases slightly in amplitude with increasing frequency. The amplitude difference of 15 dB between the D180 and D180T configurations results from the engine arrangement and the associated difference in distance to the fuselage surface itself. Overall, the surface pressure level induced by fan noise is relatively low, reaching a maximum of 90 dB with the D180T configuration. Notably, the simulation was calculated with ideal blades. A comparative simulation with a blade angle deviation of 1.5° (corresponding to an older engine) revealed a level increase of up to 8 dB. Jet noise, on the other hand, involves broadband excitation and induces significantly higher pressure levels on the fuselage surface, with pressure peaks of up to 130 dB for the D180T engine configuration.

Figure 9 shows an example of the frequency-dependent sound pressure level for the D180T configuration at 172 Hz for fan noise and jet noise. For the surfaces highlighted in dark blue, no pressure data were available. This representation does not contain any phase information and therefore provides a condensed overview of the maximum induced sound pressure level along the entire fuselage surface. While fan noise mainly radiates to the front and partly to the rear, the propagation of jet noise has omnidirectional characteristics.

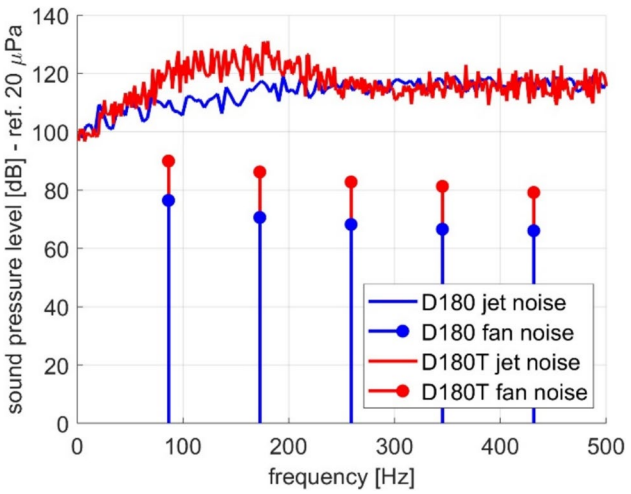

Fig. 8 Spectral analysis of the specific surface pressure excitations for the D180 and D180T configurations. The amplitudes represent the maximum surface pressure level peaks occurring over the entire fuselage for each frequency line

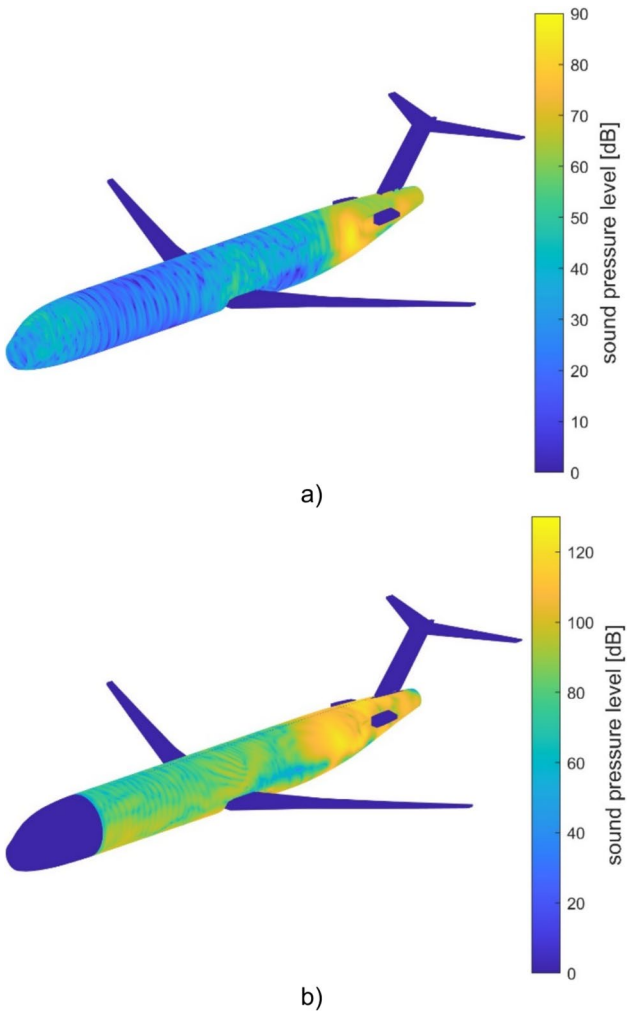

Fig. 9 Sound pressure level for the D180T configuration at 172 Hz: **a** Fan noise **b** Jet noise

4 Integrated energy analysis

For the characterization of the structural dynamic properties of complete aircraft in a vibroacoustic context, it is not beneficial to analyze individual operational deflection shapes at discrete frequencies because an enormous amount of data is generated, which makes meaningful interpretation difficult. Instead, a spatially and spectrally integrated consideration of the kinetic energy E_{kin}

$$E_{\mathrm{total}} = \int_{\Omega} \int_{S} E_{\mathrm{kin}} \, dS \, d\Omega \tag{5}$$

is carried out as part of a vibroacoustic evaluation at the primary structure level, which allows a condensed and robust characterization of the structural dynamic properties beyond the low-frequency range and is simultaneously related to the sound level in the cabin [19]. In the context of cabin noise, a large-scale energy distribution along the fuselage surface S was calculated. Here, a spatial subdivision was made between the passenger and cargo compartments not only in the circumferential direction but also in the longitudinal direction (15 areas). This concept allows a compact global evaluation of the characteristic energy distribution over the entire fuselage surface. For spectral integration over Ω, one-third octave bands commonly used in acoustics were used to provide frequency-dependent energetic averaging that provides a robust characterization of the structural dynamic vibration energy.

Figure 10 shows the spatially and spectrally integrated energy distributions for the acoustic and vibrational excitation range between 140 and 180 Hz for the D180 and D180T configurations. In this one-third octave band, the surface loads induced by the excitation are significantly higher for D180T (see Fig. 8), which ultimately also scales with the resulting energy densities. For this reason, an independent approach was chosen for both configurations to visually emphasize the specific energy distributions for both configurations in the same way.

In the D180 configuration (see Fig. 10a), an increased energy density can be observed in the central fuselage area of the passenger cabin, whereas the lowest energy level occurs in the front and rear areas of the passenger cabin. This concentrated energy distribution in the fuselage center area can be explained by the fact that the largest pressure fluctuations on the fuselage skin are induced in this area by the acoustic excitation sources, as well as by the fact that in this area, the vibration energy from the engine is transferred from the wing to the fuselage structure. In the D180T configurations (see Fig. 10b), on the other hand, the largest energy input induced by the acoustic and vibrational excitation sources occurs in the rear fuselage area. Starting from this excitation area, a characteristic energy flow is clearly recognizable along the fuselage structure.

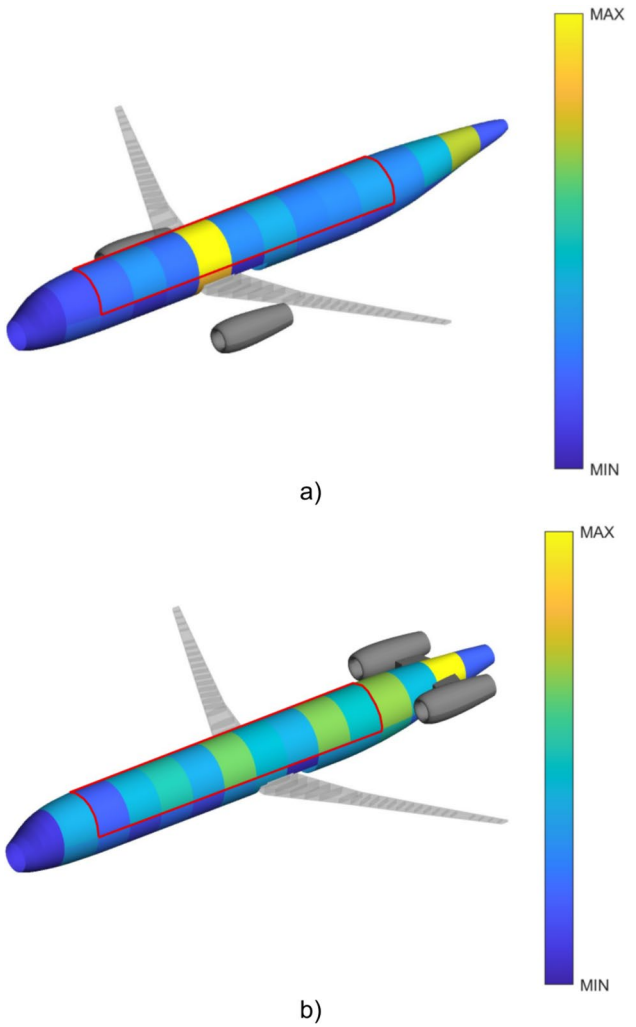

Fig. 10 Integrated energy distribution for acoustic and vibrational excitation along the fuselage surface in the frequency range from 140 to 180 Hz; the passenger cabin is outlined in red: **a** D180 configuration, **b** D180T configuration

In summary, the energy distribution for the investigated third-octave band is more balanced along the fuselage structure for the D180T configuration than for the D180 configuration. The D180 configuration, on the other hand, causes relatively high noise input in the passenger cabin near the wing-fuselage interface.

5 Conclusion

This publication covers the development of parametric primary structure models for the finite element method with the aim of creating a reliable basis for vibroacoustic cabin noise analyses. The focus here was on systematic

and generally valid modeling guidelines that follow clearly defined rules to generate consistent models. A main contribution to this was the frequency-dependent determination of the required mesh resolution of the fuselage skin in the circumferential and longitudinal directions based on a wavenumber analysis. By evaluating experimental data on the vibration behavior of a simplified A320 fuselage structure, it was possible to derive a suitable mesh resolution for frequencies up to 500 Hz. By directly comparing the wavenumber analysis with the simulated data, it was also possible to validate that the presented level of detail of the FE model has sufficient model quality to reproduce the vibration phenomena of the fuselage structure up to at least 500 Hz with good accuracy. This model accuracy is essential for comprehensive cabin noise analyses, as the acoustic excitations caused by jet engines contribute significantly to vibroacoustic noise, particularly in this frequency range.

Furthermore, it was shown that a spatially and spectrally integrated energy approach is a powerful method for characterizing vibroacoustic behavior, allowing an efficient evaluation of alternative aircraft configurations with respect to cabin noise at the primary structure level.

Especially in the context of automated model generators, the results of this work provide a methodical basis for optimized, frequency-adapted modeling of the primary structure and thus for a more precise prediction of cabin noise in early design phases.

Modern propulsion concepts, such as open-rotor engines, are characterized by their high efficiency and low fuel consumption, but at the same time, they radiate higher noise levels than conventional engines do [20]. Also, UHBR engines lead to new vibroacoustic problems, i.e., an increase in engine-induced vibration at lower frequencies. Therefore, the development of effective noise measures, such as those presented in [21], are needed in the cabin. Since subsequently implemented noise reduction measures are expensive and always accompanied by additional mass, precise cabin nose assessments will be essential in the preliminary design phase of future aircraft.

In addition to establishing common modeling guidelines to improve the accuracy of parametrically generated FE models for cabin noise analysis in the early design phase, it is also important to reduce the computational cost of such large-scale simulations. Strategies such as frequency-adaptive meshing and efficient preconditioning, as proposed by Hüpel et al. [22], contribute to this objective. Furthermore, the application of advanced numerical methods, such as Carrera's Unified Formulation proposed by Moruzzi [5], has been shown to further reduce the computational cost in vibroacoustic analyses.

Author contributions R.D.D. wrote the main manuscript text and conducted the analyses. T.K. created the fundamental models with the model generator "ModGen". C.H. revised the manuscript critically for important intellectual content. R.W. revised the manuscript critically for important intellectual content.

Funding Open Access funding enabled and organized by Projekt DEAL.

Data availability Acoustic Flight-Lab measurement data analyzed in this study are subject to a Data Use Agreement and cannot be made available. Selected datasets generated during this study are available from the corresponding author on reasonable request.

Declarations

Conflict of interest The authors declare no competing interests.

References

1. Hesse, C., Allebrodt, P., Teschner, M., Biedermann, J.: Knowledge-based model generation for aircraft cabin noise prediction from pre-design data. CEAS Aeronaut. J. **15**, 1127–1136 (2024). https://doi.org/10.1007/s13272-024-00769-z
2. Winter, R., Biedermann, J., Norambuena, M.: High-resolution vibration measurement and analysis of the Flight-LAB aircraft fuselage demonstrator. In: INTER-NOISE 2018–47th International Congress and Exposition on Noise Control Engineering: Impact of Noise Control Engineering (2018)
3. Hesse, C., Dewald R. D., Allebrodt P., Winter R., Biedermann J.: Sensitivitätsanalyse für die numerische Vorhersage von Kabinenlärm in Flugzeugen. In: DAGA 2024 - 50. Jahrestagung für Akustik (2024). https://elib.dlr.de/204156/
4. Blech, C., Appel, C., Ewert, R., Delfs, J., Langer, S.: Wave-resolving numerical prediction of passenger cabin noise under realistic loading. In: Radespiel, R., Semaan, R. (eds.) Fundamentals of high lift for future civil aircraft: contributions to the final symposium of the collaborative research center 880, December 17–18, 2019 Braunschweig, Germany, vol. 145, pp. 231–246. Springer International Publishing, Berlin (2020). https://doi.org/10.1007/978-3-030-52429-6_15
5. Moruzzi, M. C.: Vibro-acoustic analysis and design optimization to improve comfort and sustainability of future passenger aircraft. PhD thesis, Università di Bologna (2023). https://doi.org/10.48676/unibo/amsdottorato/10700
6. Joshi, P., Mulani, S. B., Kapania R. K.: Vibroacoustic studies on structurally optimized Pareto designs of curved composite stiffened panel. In: AIAA SCITECH 2024 Forum (2024). https://doi.org/10.2514/6.2024-0769

7. Sinha, K., Klimmek, T.: A framework for the bi-level optimization of a generic transport aircraft fuselage using aeroelastic loads. CEAS Aeronaut. J. (2023). https://doi.org/10.1007/s13272-022-00628-9
8. Klimmek, T.: Parameterization of tolopogy and geometry for the multidisciplinary optimization of wing structure. In: CEAS 2009 - Euopean Air and Space Conference (2009)
9. Alder M., Moerland, E., Jepsen, J., Nagel, B.: Recent advances in establishing a common language for aircraft design with CPACS. In: Aerospace Europe Conference 2020 (2020). https://elib.dlr.de/134341/
10. Biedermann, J., Winter, R., Norambuena Gonzalez, M., Böswald, M.: Classification of the mid-frequency range based on spatial Fourier decomposition of operational deflection shapes. In: 24th International Congress on Sound and Vibration (ICSV24) (2017). https://doi.org/10.25144/24122
11. Hambric, S., Fahnline, J.: Structural acoustics tutorial – Part 2: sound-structure interaction. Acoust. Today. **3**(2), 9–25 (2007). https://doi.org/10.1121/1.2961152
12. Marburg, S.: Six boundary elements per wavelength: is that enough? J. Comput. Acoust. **10**(1), 25–51 (2002). https://doi.org/10.1142/S0218396X02001401
13. Langer, P., Maeder, M., Guist, C., Krause, M., Marburg, S.: More than six elements per wavelength: the practical use of structural finite element models and their accuracy in comparison with experimental results. J. Comput. Acoust. (2017). https://doi.org/10.1142/S0218396X17500254
14. DLR, "INTONATE," Institute of Aeroelasticity, [Online]. Available: https://www.dlr.de/en/ae/research-transfer/projets/intonate. [Accessed 10 March 2025].
15. Lummer, M.: A hybrid 3D discontinuous Galerkin code for CAA applications. In: 22nd AIAA/CEAS Aeroacoustics Conference (2016). https://doi.org/10.2514/6.2016-2719
16. Blech, C., Appel, C.K., Ewert, R., Delfs, W.J.: Numerical prediction of passenger cabin noise due to jet noise by an ultra–high–bypass ratio engine,". J. Sound Vibr. (2020). https://doi.org/10.1016/j.jsv.2019.114960
17. Ewert, E., Dierke, J., Siebert, J., Neifeld, A., Appel, C., Siefert, M., Kornow, O.: CAA broadband noise prediction for aeroacoustic design. J. Sound Vib. **330**(17), 4139–4160 (2011). https://doi.org/10.1016/j.jsv.2011.04.014
18. Zettel, S. F., Böswald, M., Dewald R. D., Winter, R.: Jet engine vibration model for estimating pylon-wing interface loads for realistic structural excitation. In: Deutscher Luft- und Raumfahrt Kongress (2024).
19. Biedermann, J., Winter, R., Wandel, M., Böswald, M.: Energy based correlation criteria in the mid-frequency range. J. Sound Vib. **400**, 457–480 (2017). https://doi.org/10.1016/j.jsv.2017.04.024
20. Wei, Q., Chen, Z., Tong, F., Li, G., Cui, P.: Numerical simulation of noise characteristics of open rotor. J. Phys. Conf. Ser. (2022). https://doi.org/10.1088/1742-6596/2280/1/012058
21. Ajith, A., Balakrishnan, B., Raja, S., Paul Vizhian, S.: Sound transmission performance of plate-type acoustic metamaterials for quieter aircraft cabins. Appl. Acoust. (2025). https://doi.org/10.1016/j.apacoust.2025.110806
22. Hüpel, Y., Blech, C., Sreekumar, H.K., Langer, S.C.: Efficient solutions of preconditioned large-scale systems for simulative aircraft cabin noise assessment. PAMM (2023). https://doi.org/10.1002/pamm.202300102